J MATER SCI **41** (2006) 2615–2619

Structural investigation of Ge–Sb–Sn thin films using transmission electron microscopy

M. NAITO*, M. ISHIMARU, Y. HIROTSU
The Institute of Scientific and Industrial Research, Osaka University, Mihogaoka, Ibaraki, Osaka 567-0047, Japan
E-mail: naito22@sanken.osaka-u.ac.jp

M. TAKASHIMA, H. MATSUMOTO
Science and Technology Research Center, Inc., Mitsubishi Chemical Group, Kamoshida-cho, Aoba-ku, Yokohama, Kanagawa 227-8502, Japan

Published online: 17 April 2006

Atomistic structures of as-deposited and laser-induced-crystallized Ge–Sb–Sn layers have been examined using high-resolution electron microscopy (HREM) and nanobeam electron diffraction (NBED). Cross-sectional observations were performed on Ge–Sb–Sn thin films embedded in a multi-layered structure. Crystalline clusters were frequently observed in the HREM images of the as-deposited amorphous Ge–Sb–Sn thin film. Autocorrelation function analysis of the HREM image indicated a similarity between the structures of the crystalline clusters and that of rhombohedral Sb. Atomic pair-distribution functions obtained from the halo NBED intensity of the as-deposited amorphous Ge–Sb–Sn films also showed development of local structure whose atomic configuration is similar to that of the rhombohedral Sb. NBED revealed that the structure of the crystallized Ge–Sb–Sn thin film is also close to that of rhombohedral Sb. The atomistic structures of Ge–Sb–Sn thin films were compared with those of Ge–Sb–Te thin films and the rapid crystallization mechanism of these materials was discussed.

1. Introduction

With the advance of information technology, large-sized digital data, sometimes over several gigabytes, have been used. As a result, data storage with a high density and a high-recording speed is required. Rewritable optical disks such as DVD-RW or DVD-RAM are mature data storage devices satisfying these demands. In these optical disks, information is recorded by taking advantage of the difference in the optical properties such as reflectance and transmittance between the amorphous and the crystalline phases of a recording material. Reversible amorphous-to-crystalline phase-change can be achieved by the irradiation of a well-focused laser beam. In this technique, sub-micron sized amorphous areas surrounded by the crystalline phase act as data bits. Therefore one way to enhance the recording capacity is the formation of smaller amorphous areas. Since the recording speed strongly depends on the crystallization rate of the recording material, much effort has been devoted to find materials which crystallize within a short time, no longer than several tens of nanoseconds.

In contrast with the development of recording speed and recording capacity, the recording mechanism remains an open question. This situation may be attributed to the complex microscopic structure of phase-change disks, as is the case for other real devices. In phase-change disks, the thickness of the recording layer is less than 20 nm. Besides, the recording layer is sandwiched between protective layers. These make it difficult to investigate the recording materials in the real disks directly. Instead of real phase-change disks, some researchers prepared thick films of phase-change materials deposited on a glass or other substrate for the purpose of structural analyses and/or physical property studies. However, this method is not always the best way to study the characteristics of materials embedded in real devices.

*Author to whom all correspondence should be addressed.
0022-2461
DOI: 10.1007/s10853-006-7821-z

The development of methods to investigate the materials included in such a real device is extremely important. Cross-sectional observation using transmission electron microscopy (TEM) in combination with high-resolution electron microscopy (HREM) and nanobeam electron diffraction (NBED) technique [1] is a powerful technique for analyzing the local structure of recording materials embedded in a phase-change optical disk.

Currently, $GeTe–Sb_2Te_3$ pseudobinary compounds [2] are widely applied to phase-change materials because of their rapid crystallization speed, sufficient difference in optical constants between the amorphous and crystalline phases, high thermal stability of amorphous recording marks, and enough durability for overwriting. In addition to these materials, some Sb-rich alloys [3–6] become candidates for high-speed phase-change recording materials. Among them, a Ge–Sb–Sn ternary alloy is thought to be suitable for high-speed phase-change recording. However, crystalline and amorphous structures of Ge–Sb–Sn have not been examined yet. In this study, we carried out the microstructural analysis of as-deposited and laser-induced crystalline phases of a Ge–Sb–Sn thin film embedded in a multi-layered structure using HREM and NBED for the first time.

2. Experimental

The samples used in the present study have a multi-layered structure consisting of a reflective layer (Ag, ∼200 nm), an upper protective layer ($ZnS–SiO_2$, ∼40 nm), a recording layer (Ge–Sb–Sn, ∼20 nm), and a lower protective layer ($ZnS–SiO_2$, ∼90 nm). This multi-layered structure is similar to that of a conventional phase-change optical recording medium. Thin films of Ag, $ZnS–SiO_2$, and Ge–Sb–Sn were grown at room temperature onto a pre-grooved polycarbonate substrate by a sputtering method. The recording layer had the composition, in terms of atomic ratio, of Ge:Sb:Sn ∼ 1:7:2. The crystalline Ge–Sb–Sn thin film was obtained by laser-annealing of the as-deposited sample. Cross-sectional TEM samples were prepared as follows. A single crystalline Si wafer was glued onto the lower protective layer after the multi-layer was exfoliated from the polycarbonate substrate successfully by adhesive tape. The adhesive tape was removed using acetone, and the multi-layer was sandwiched between two pieces of Si wafers by gluing an additional Si wafer to the reflective layer. This sandwiched sample was mechanically polished using a tripod polishing technique, followed by argon ion thinning at a low accelerating voltage (2 keV) with a low glancing angle (4°) to thin down the sample. Atomistic structures of Ge–Sb–Sn thin films were observed using JEOL JEM-3000F and JEOL JEM-2010 electron microscopes operated at 200 kV. NBED patterns and TEM images were recorded on imaging plates, which had a higher sensitivity and a wider dynamic range for electron-beam intensities compared to the conventional TEM films [7]. The electron probe size in NBED was as small as 10 nm in diameter.

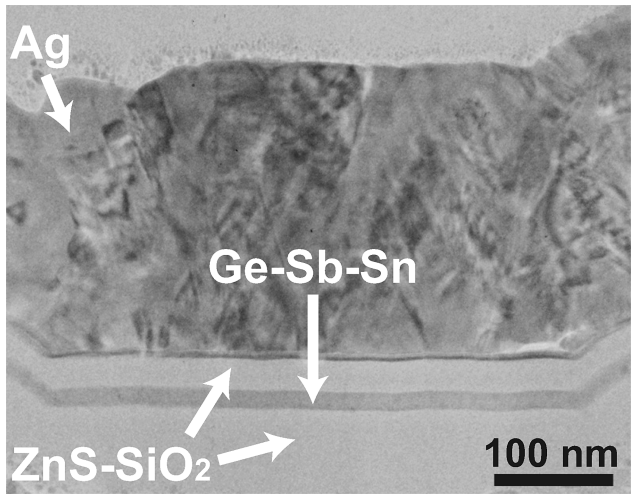

Figure 1 Cross-sectional bright field image of the as-deposited specimen. The multi-layered structure can be seen clearly. The gray layer with a thickness of approximately 20 nm corresponds to the Ge–Sb–Sn thin film.

3. Results and discussion

Fig. 1 shows a cross-sectional bright field TEM image of the as-deposited specimen around the grooved area. The horizontal direction of the TEM image corresponds to the radial direction of the phase-change disk. The cross-sectional specimen was prepared successfully, and the multi-layered structure can be seen clearly due to the difference in the image contrast. The darker contrast region with a thickness of ∼20 nm corresponds to the Ge–Sb–Sn thin film (indicated by an arrow). To obtain information on atomistic structures of the Ge–Sb–Sn thin film, HREM observations were performed. In the HREM image shown in Fig. 2a, the middle darker contrast region between the dotted lines corresponds to the Ge–Sb–Sn thin film. The NBED pattern obtained from the Ge–Sb–Sn thin film region is also shown in the inset. The "salt and paper" contrast in the HREM image and the halo diffraction pattern indicate that the as-deposited Ge–Sb–Sn thin film possesses an amorphous structure. A close examination of the HREM image revealed crystalline atomic clusters as small as 2 or 3 nm in the amorphous matrix, as shown by white circles. In our previous study [8, 9], the crystalline clusters were also observed in the as-deposited amorphous Ge–Sb–Te thin film as shown in Fig. 2b. Compared with the as-deposited Ge–Sb–Te thin film, it seems that the crystalline clusters in the as-deposited Ge–Sb–Sn thin film were observed more frequently and were more developed in size. In other words, the as-deposited Ge–Sb–Sn thin film is more ordered than the as-deposited Ge–Sb–Te thin film. We discuss the structural differences in these thin films more quantitatively in the last part of this section.

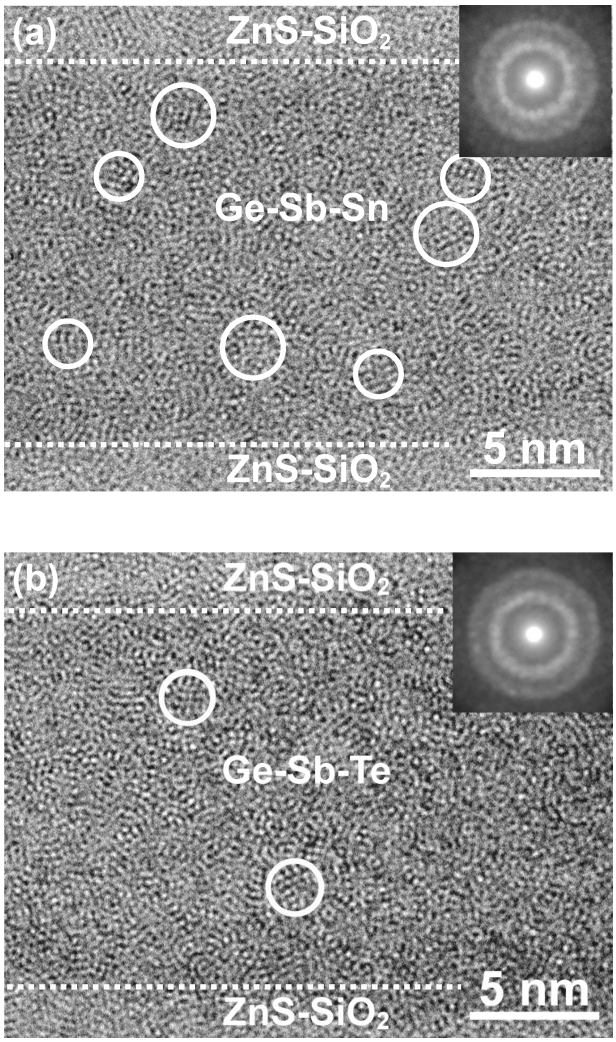

Figure 2 Cross-sectional HREM image of the (a) as-deposited Ge–Sb–Sn and (b) as-deposited Ge–Sb–Te thin film. In the regions with white circles the crystalline clusters are observed. NBED patterns obtained from the Ge–Sb–Sn and Ge–Sb–Te thin films are also shown in the inset.

To investigate the structure of the crystalline clusters in the as-deposited Ge–Sb–Sn thin film, the autocorrelation function (ACF) analysis [10] was performed for HREM images. The resultant ACF images from two different regions are shown in Fig. 3a and b. Judging from the lattice fringe spacings and cross angles of these ACF images, we concluded that the structure of the crystalline clusters is close to that of rhombohedral Sb (space group: $R\bar{3}m$, and lattice parameters: $a = 0.431$ nm, $c = 1.13$ nm) [11]. Simulated HREM images of rhombohedral Sb with zone axes of $[2\bar{2}01]$ and $[11\bar{2}0]$ are shown in Fig. 3c and d. The ACF images in Fig. 3a and b are consistent with the simulated images in Fig. 3c and d, respectively.

To obtain more information on the amorphous structure of Ge–Sb–Sn thin film, electron diffraction pair-distribution function analysis [12] was performed. The reduced interference function, $F(Q) = Qi(Q)$, was calculated from the NBED intensity profile. The symbol Q

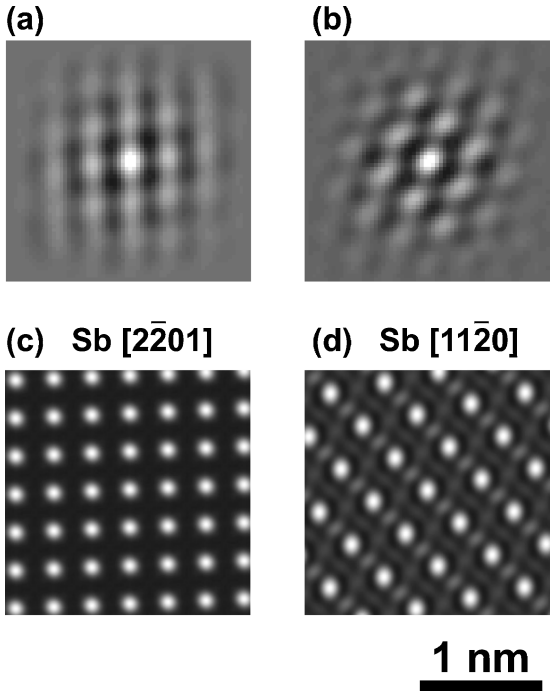

Figure 3 (a), (b) ACF images obtained from the crystalline clusters observed in HREM image of the as-deposited Ge–Sb–Sn thin film. (c), (d) Simulated HREM images of rhombohedral Sb with the $[2\bar{2}01]$ and $[11\bar{2}0]$ zone axes, respectively. The fringe spaceings and cross angles of ACF images are close to those obtained from the simulated HREM images.

represents the scattering vector expressed as $Q = 4\pi \sin\theta/\lambda$, where θ is the half-scattering angle and λ the wavelength of incident electrons. The interference function $i(Q)$ was extracted from the averaged electron intensity profile, $\langle I(Q)\rangle$, by drawing smooth background curve linking the middle points between the intensity maxima and minima of the halo-intensity profile. The $F(Q)$ profile of the as-deposited Ge–Sb–Sn thin film is recorded as high as $Q = 200$ nm^{-1} (Fig. 4a). The $F(Q)$ is related to the reduced radial distribution function $G(r)$ by the Fourier transform as

$$G(r) = \frac{2}{\pi}\int_0^\infty F(Q)\sin(Qr)dQ = 4\pi r[\rho(r) - \rho_0],$$

where r is the radial distance, $\rho(r)$ the atomic density, and ρ_0 the average atomic density. The atomic pair-distribution function $g(r) = G(r)/4\pi r\rho_0 + 1$ is indicated in Fig. 4b. The bars on the abscissa represent the interatomic distances found in crystalline Sb. The first main peak is centered at 0.287 nm and this value is in agreement with the first-nearest-neighbor distance of amorphous Sb [13]. This value is also close to the inteatomic distance of 0.290 nm found in rhombohedral Sb [11]. On the other hand, the second peak consists of some shoulders and small humps. The small peaks and shoulders indicated by triangles are in good agreement with the interatomic distances of 0.336, 0.431, and 0.547 nm found in rhombohedral Sb, suggesting that the atomic configuration

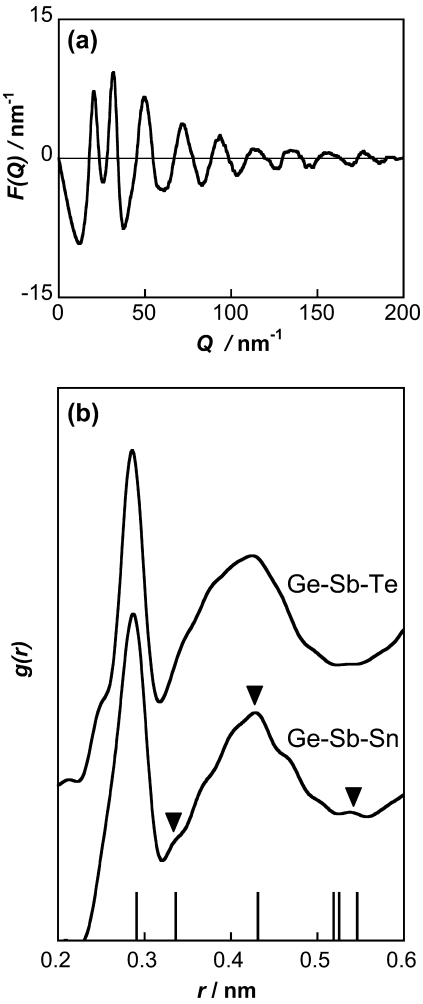

Figure 4 (a) Reduced interference function $F(Q)$ and (b) atomic pair-distribution functions $g(r)$ profiles for as-deposited Ge–Sb–Sn thin film and as-deposited Ge–Sb–Te thin film. The bars on the abscissa in (b) indicate the interatomic distances found in rhombohedral Sb.

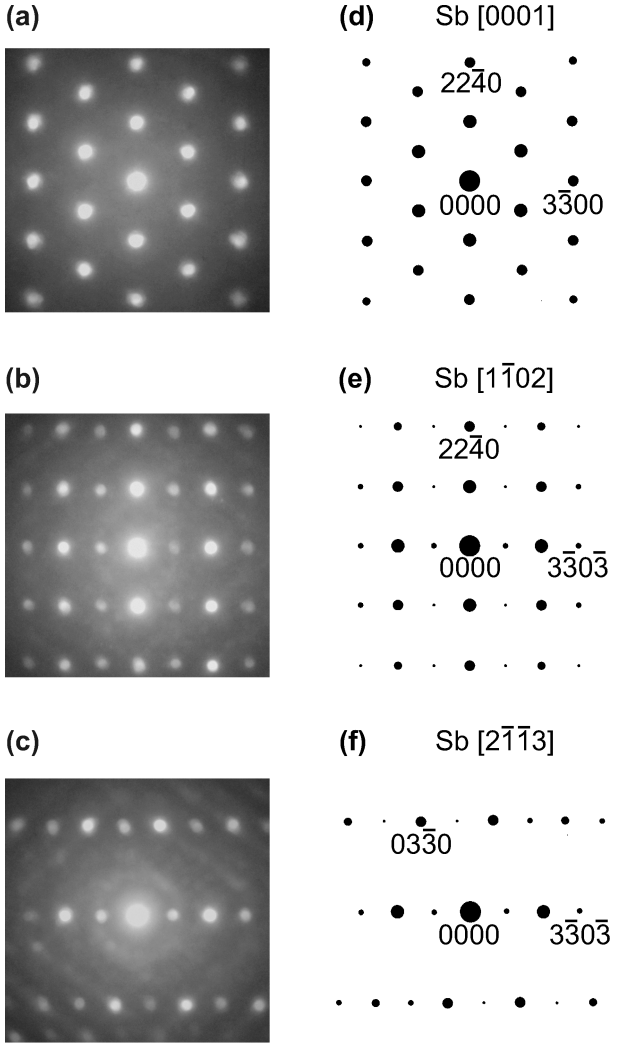

Figure 5 (a)–(c) show the NBED patterns obtained from the laser-induced crystalline phase of the Ge–Sb–Sn thin film. (d)–(f) show the simulated electron diffraction patterns from rhombohedral Sb with zone axes of [0001], [1$\bar{1}$02], and [2$\bar{1}\bar{1}$3], respectively.

originated from rhombohedral Sb exists in the as-deposited Ge–Sb–Sn thin film. This result is consistent with ACF analysis.

Presuming that the crystalline clusters in the amorphous phase affects the rapid crystallization of this material, a structural relation between the crystalline clusters in the amorphous Ge–Sb–Sn and the crystalline Ge–Sb–Sn was investigated using NBED. The result showed that the structure of the laser-induced crystalline phase of Ge–Sb–Sn is similar to that of rhombohedral Sb. Fig. 5a–c display the NBED patterns obtained from the laser-induced crystalline phase of the Ge–Sb–Sn thin film. From the calculation based on the kinematical scattering approximation, it is found that these NBD patterns correspond to the [0001], [1$\bar{1}$02], and [2$\bar{1}\bar{1}$3] net patterns of rhombohedral Sb (see Fig. 5d–f). Taking the similarity between the structure of the crystalline phase of Ge–Sb–Sn and that of rhombohedral Sb into account, this result also implies the structural similarity between crystalline clusters existing in the amorphous phase and the crystalline phase of the Ge–Sb–Sn thin film. These results indicate that the amorphous structure of the Ge–Sb–Sn thin film is ready for the amorphous-to-crystalline phase-change.

Finally, we compare the atomistic structure of the Ge–Sb–Sn thin film with that of the Ge–Sb–Te thin film reported previously [8, 9]. As described above, HREM observations indicated that the crystalline clusters in the as-deposited amorphous Ge–Sb–Sn thin film are more developed compared with the as-deposited Ge–Sb–Te thin film. This tendency is also confirmed in $g(r)$. The $g(r)$ obtained from the as-deposited Ge–Sb–Te thin film is shown in Fig. 4b. The distinct difference between $g(r)$s in Fig. 4 can be seen in the second peak: the small peaks and shoulders related to the local development of crystalline atomic clusters become more pronounced in the $g(r)$ of the as-deposited Ge–Sb–Sn thin film than that of

the as-deposited Ge–Sb–Te thin film. The Ge–Sb–Sn thin films have the property of high-speed recording equal to or higher than that of the Ge–Sb–Te thin film, suggesting that the number or size of the crystalline clusters in the amorphous phase would be related to the crystallization property. The structural similarity based on the atomic configuration of rhombohedral Sb between amorphous and crystalline phase were considered to be responsible for the rapid crystallization of Sb-rich phase-change materials.

4. Conclusions

We performed atomistic structural analysis of the as-deposited amorphous phase and the laser-induced crystalline phase of a Ge–Sb–Sn thin film embedded in a multi-layered structure. The as-deposited Ge–Sb–Sn thin film possesses the amorphous phase in which crystalline atomic clusters are frequently observed. The ACF images obtained from HREM images revealed the structural similarity between crystalline clusters and rhombohedral Sb. In addition, the small peaks and shoulders were observed at $r \sim 0.336$, 0.431, and 0.547 nm in $g(r)$ obtained from the as-deposited Ge–Sb–Sn thin film indicating that the atomic configuration similar to rhombohedral Sb exists. On the other hand, the structural similarity between the laser-induced crystalline phase of the Ge–Sb–Sn thin film and crystalline Sb is also detected by NBED. That is, both the structures of the crystalline clusters in the amorphous Ge–Sb–Sn and of the crystalline Ge–Sb–Sn are similar to that of the rhombohedral Sb. It is considered that the rapid crystallization of the Sb-rich materials may be correlated with the structural similarity before and after the crystallization.

Acknowledgments

The authors are grateful to Masae Kubo at Mitsubishi Chemical Co. for preparing specimens, and to Takeshi Ishibashi at ISIR, Osaka Univ. for preparing TEM specimens. This work was partly sponsored by 21st Century Center of Excellence (COE) program, Grant-in-Aid for Scientific Research (#16560008) and the Murata Science Foundation.

References

1. Y. HIROTSU, M. ISHIMARU, T. OHKUBO, T. HANADA and M. SUGIYAMA, *J. Electron Microsc.* **50** (2001) 435.
2. N. YAMADA, E. OHNO, K. NISHIUCHI, N. AKAHIRA and M. TAKAO, *J. Appl. Phys.* **69** (1991) 2849.
3. M. HORIE, T. OHNO, N. NOBUKUNI, K. KIYONO, T. HASHIZUME and M. MIZUNO, *Proc. SPIE* **4342** (2002) 76.
4. J. P. CALLAN, A. M.-T. KIM, C. A. D. ROESER, E. MAZUR, J. SOLIS, J. SIEGEL and C. N. AFONSO, *Phys. Rev. Lett.* **86** (2001) 3650.
5. L. VAN PIETERSON, M. VAN SCHIJNDEL, J. C. N. RIJPERS and M. KAISER, *Appl. Phys. Lett.* **83** (2003) 1373.
6. B. J. KOOI and J. TH. M. DE HOSSON, *J. Appl. Phys.* **95** (2004) 4714.
7. N. MORI, T. OIKAWA, Y. HARADA and J. MIYAHARA, *J. Electron Microsc.* **39** (1990) 433.
8. M. NAITO, M. ISHIMARU, Y. HIROTSU and M. TAKASHIMA, *Jpn. J. Appl. Phys.* **42** (2003) L1158.
9. *Idem. J. Appl. Phys.* **95** (2004) 8130.
10. J. FRANK, "Computer Processing of Electron Microscopy" (Springer, Berlin, 1980) p. 187.
11. P. VILLARS and L. D. CALVERT, "Pearson's Handbook of Crystallographic Data for Intermetallic Phases" (American Society for Metals, Ohio, 1985) Vol. 3.
12. T. OHKUBO and Y. HIROTSU, *Phys. Rev.* **B 67** (2003) 094201.
13. V. H. RICHTER, H. BERCKHEMER and G. BREITLING, *Z. Naturf.* **9a** (1954) 236.